

Supporting Information

Elucidating the Role of Heterojunction Interface in Exciton Harvest and Charge Collection of Organic Solar Cells through Planar Heterojunction Structure

Quanbin Liang, Yuan Xie* and Hongbin Wu*

Institute of Polymer Optoelectronic Materials and Devices, State Key Laboratory of Luminescent Materials and Devices, South China University of Technology, Guangzhou, 510640, P. R. China.

*E-mail: xieyuan@scut.edu.cn, hbwu@scut.edu.cn

1. Methods

1.1 Device Fabrication

BHJ device: The BHJ device structure is ITO/ZnO/J52:IEICO-4F/MoO₃/Ag. The devices were fabricated on indium tin oxide (ITO) coated glass substrates (Nanbo Glass Inc., Shenzhen, P. R. China) with sheet resistance of 15Ω per square. The ITO substrates were cleaned by a surfactant scrub, followed by a series of wet cleaning in acetone and isopropanol inside ultrasonic bath, then dried in an oven. The ZnO precursor solution was spin-cast on top of the ITO-glass substrate. The films were annealed at 200 °C for 30 min in air. The thickness was approximately 40 nm. The ZnO-coated substrates were transferred into a glove box. The J52: IEICO-4F bulk heterojunction active layer, with nominal thickness around 100 nm, was prepared by spin-coating the mixed solvent of chlorobenzene/1,8-diiodooctane (DIO) (99.5%: 0.5% by volume) solution (with a total concentration of 20 mg ml⁻¹) at 1300 r.p.m. for 1 min in a nitrogen filled glove box (O₂ < 1 ppm, H₂O < 1 ppm). The films were heated at 160°C for 10 min. Then, a thin layer of MoO_x film (≈8 nm) was evaporated on top of the active layer. Finally, the anode (Ag, ≈100 nm) was deposited through a shadow mask by thermal evaporation in a vacuum with a pressure of 1×10⁻⁴ Pa. The active area of device was 4.5 mm² in a vacuum chamber.

PHJ device: The PHJ device structure is ITO/ZnO/IEICO-4F//J52/MoO₃/Ag. First, a film with the structure of glass/PEDOT:PSS/J52 was prepared by successive spin coating of an aqueous solution of PEDOT:PSS and a chlorobenzene solution of J52.

This J52 film was lightly contacted onto a device with a structure of ITO/ZnO/IEICO-4F. 1 drop of water was placed on the edge of the stacked substrates. The water selectively penetrated into the PEDOT:PSS layer. After the PEDOT:PSS layer was completely dissolved, the glass substrate was easily detached from the organic layer, resulting in the transfer of the J52 film from the glass to the IEICO-4F based device so as to form a PHJ active layer. Then the MoO_x and Ag were deposited to form metal electrode.

1.2 Device Characterization and measurements.

J–V characteristics were acquired using a Keithley 2400 Source Measure Unit under 1 sun, AM 1.5G (air mass 1.5 global) illumination provided by a 3A solar simulator (SAN-EI Inc., Model: XES-40S1). The illumination intensity used throughout was around 1000 W m⁻², as determined by a mono-crystal silicon reference cell (Hamamatsu S1133, with KG-5 visible color filter) calibrated by the National Renewable Energy Laboratory (NREL). Masks made from laser beam cutting technology with well-defined area size of 16.0 mm² are attached to define the effective area for accurate measurement.

EQE: The EQE spectra were measured by a solar cells–photodetector responsivity measurement system (Enlitech Inc.), which was calibrated with a certified mono-crystal silicon reference cell. The sub-bandgap EQE spectra were obtained using the same system operated under high sensitivity mode, with a highly sensitive pre-amplifier.

TPV/TPC: Transient Photovoltage (TPV) and Photocurrent (TPC) measurements

were carried out following a well-established experimental setup¹. Charge carriers were generated by a laser pulse excitation at 532 nm, with a pulse width of 8 ns at a frequency of 20 Hz from an Nd: YAG solid nanosecond pulse laser (Q-smart 100 of Quantel). For TPV measurement, the signal was recorded by a Tektronix DPO4014 oscilloscope with 1M Ω input impedance under open-circuit condition. The V_{OC} of the devices were tuned by adjusting the illumination intensity of a 100 W bromine tungsten lamp through the use of neutral density filters, producing steady-state illumination intensity between 10 and 1000 W m⁻² (corresponding to 0.01–1.0 sun). For TPC measurement, solar cell devices were in series with a 50 Ω load resistor and voltage transient across the resistor was recorded by the oscilloscope under the same illumination and laser perturbation. The transient is translated into a current transient by Ohm's law. The photo-generated charge ΔQ by laser perturbation is the time-integrated current transient. All transient data consist of 128 voltage transient averaged together to counteract the fluctuation of laser pulse.

We carried out the transient photovoltage (TPV) and transient photocurrent (TPC) techniques to measure the charge carrier density and together with their lifetime,² which are the most important parameters to characterize charge carrier recombination dynamics. TPV measurements monitor the transient photovoltage decay generated by a small laser pulse during various constant bias light, enabling us to determine the charge carrier lifetimes corresponding to different open circuit voltages. TPC is measured with identical laser and bias light but under short circuit condition. Combined with TPV, charge carrier density and lifetime can be obtained

based on differential charging principle. However, there are important differences between PHJ and BHJ when solving the charge carrier density and lifetime with the TPV and TPC data.

The typical OPV devices can be viewed as variable capacitors with various bias light intensity. We can acquire the differential capacitors due to various bias light so as to extract the average charge carrier density in active layer n_{AL} under various bias voltage:

$$n_{AL} = \frac{1}{Ade} \int_0^{V_{oc}} [C_{DC}(V) - C_0] dV \quad (2)$$

Noted that the measured capacitance C_{DC} should be subtracted by a geometric capacitance C_0 due to the plate electrode to obtain the differential capacitance C_{diff} . A is the effective cell area, e is the elementary charge and d is the thickness of the active layer.

For BHJ, d is the actual thickness of the active layer because the electrons and holes are distributed randomly throughout the active layer. While for PHJ, the holes (electrons) are primarily confined within the donor (acceptor) materials, so we have taken d to be the thickness of donor layer, meaning these n values represent average hole densities.

In addition to charge density, recombination lifetime of the charge carriers should also be carefully corrected for PHJ devices, unlike the BHJ. For BHJ, differential capacitance C_{diff} is much larger than the geometric capacitance. The total carrier lifetime τ_{AL} can be expressed as: $\tau_{AL} = \tau_{\Delta n} * \delta$, where δ is the reaction order and it can be obtained by calculation.³ But for PHJ, differential capacitance is very

close to geometric capacitance or even smaller, so we have to exclude the effect of electrode charge following: $\tau_{AL} = \left(\frac{C_{diff}}{C_{diff} + C_0} \right) \tau_T$, where τ_T is the “total” lifetime of all carriers within the active layer and on the electrodes.⁴

Optical Simulation: We calculated light absorption profiles in the multilayered films by using the optical transfer matrix formalism following a reported procedure.^{5,6} The optical constants of the organic materials, MoO₃, ITO, and glass were obtained by spectroscopic ellipsometry. The optical constant of Ag was taken from a materials database. The large parasitic absorptions of the ITO/glass substrate and the Ag electrode in the OSC spectra in the 300–400 and 700–900 nm regions are visible.

2. Supplementary Figures

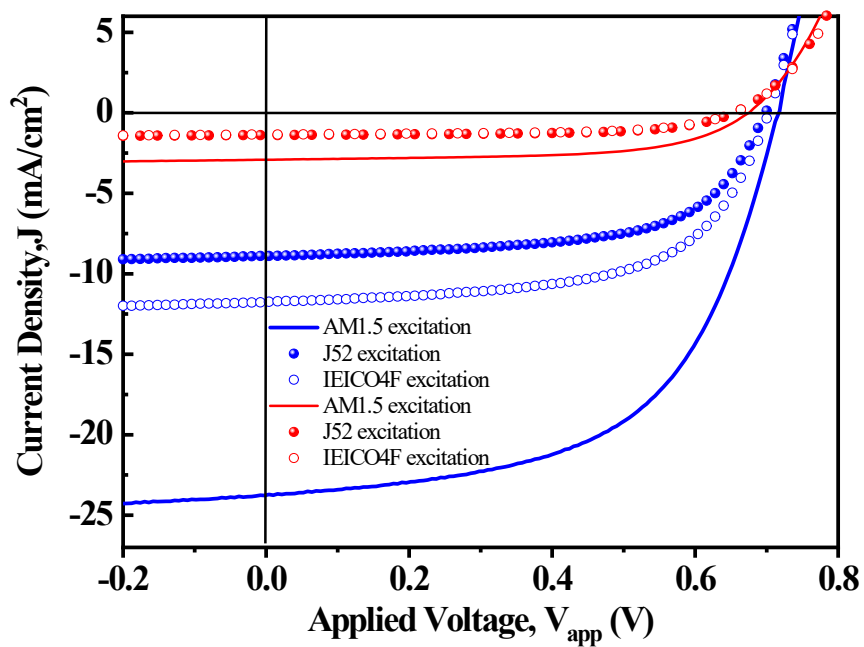


Fig. S1 Current-Voltage characteristics for both the PHJ (red) and BHJ (blue) under AM 1.5G illumination (solid line), short-wavelength illumination with a filter that only allows light below 620nm to pass (solid circle), long-wavelength illumination with a filter that only allows light above 620nm to pass (hollow circle).

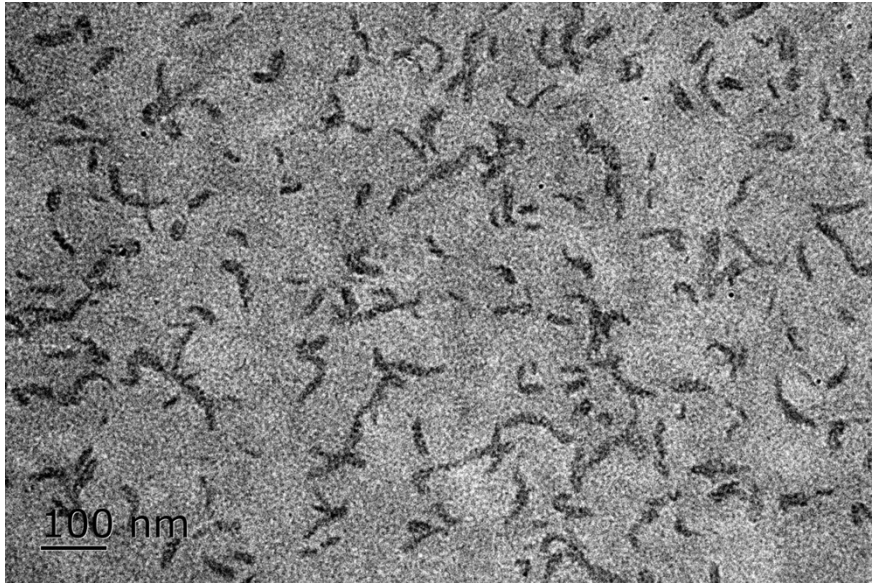
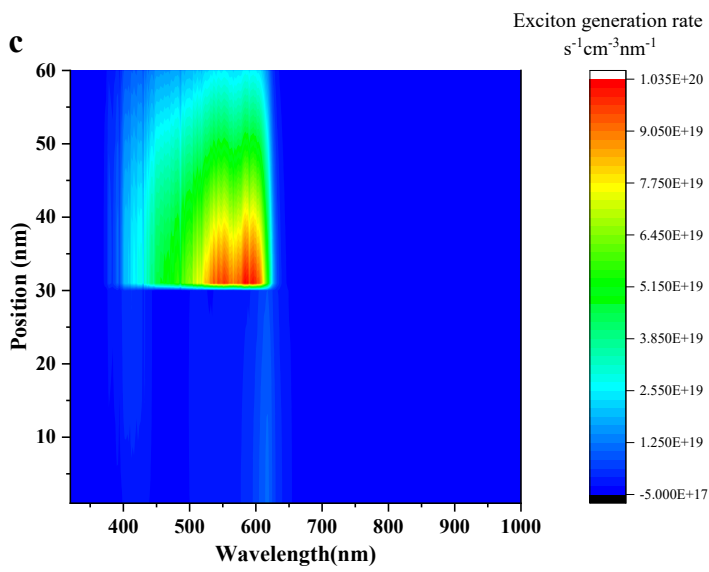
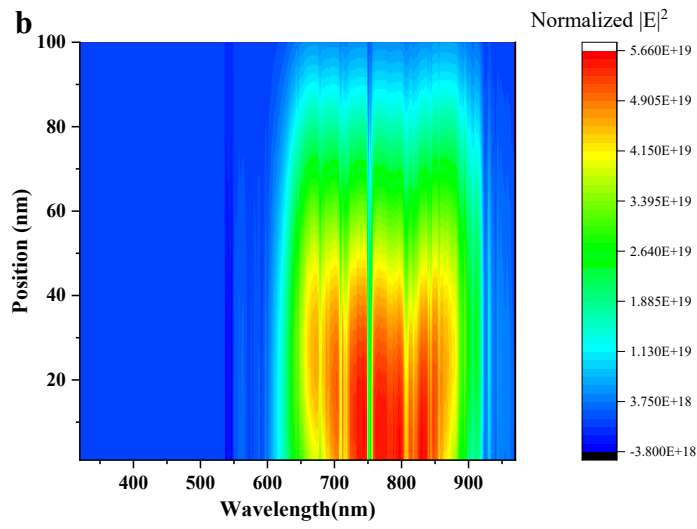
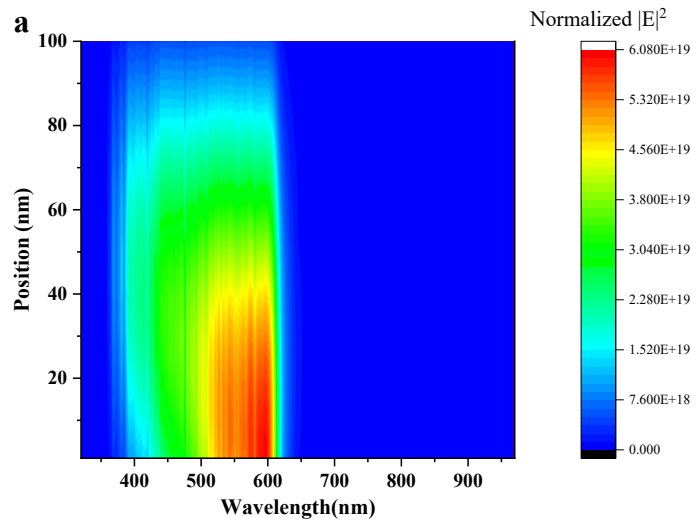


Fig. S2 Transmission electron microscope (TEM) image of the J52: IEICO-4F blend film



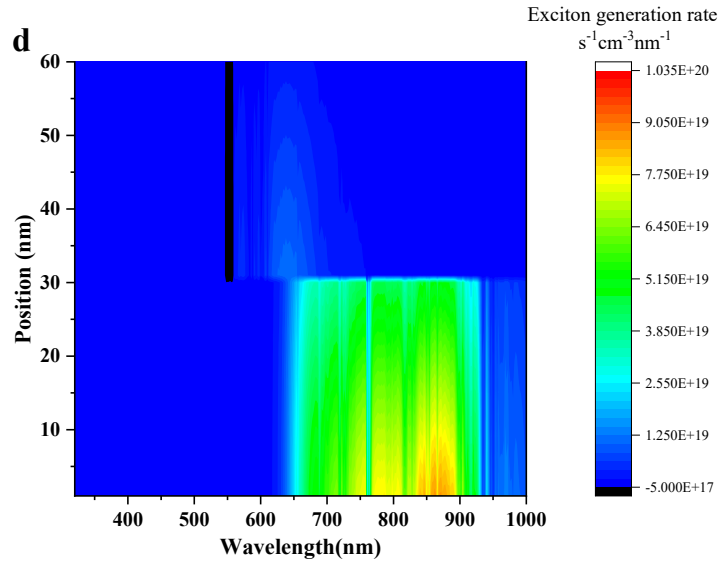


Figure S3. Calculated exciton generation rate profile $G(\lambda, z)$ for BHJ and PHJ device. $G(\lambda, z)$ as a function of wavelength and position in the active layer for BHJ (a) and '30 nm/30 nm' PHJ device (c) under short-wavelength illumination with a filter that only allows light below 620nm to pass is shown. Besides, $G(\lambda, z)$ for BHJ (b) and '30 nm/30 nm' PHJ device (d) under long-wavelength illumination with a filter that only allows light above 620nm to pass is shown. The sunlight enters from the bottom (ITO) side and hits the acceptor layer first.

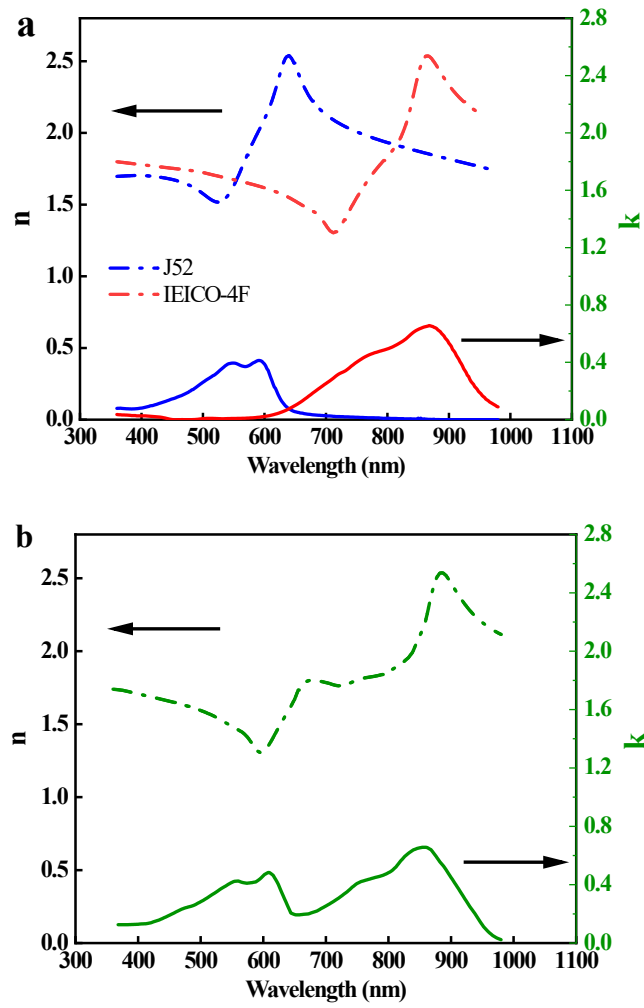


Fig. S4 Optical constants including refractive index (n) and extinction coefficient (k) of **(a)** pure J52 film, pure IEICO-4F film and **(b)** BJJ film measured by spectroscopic ellipsometry.

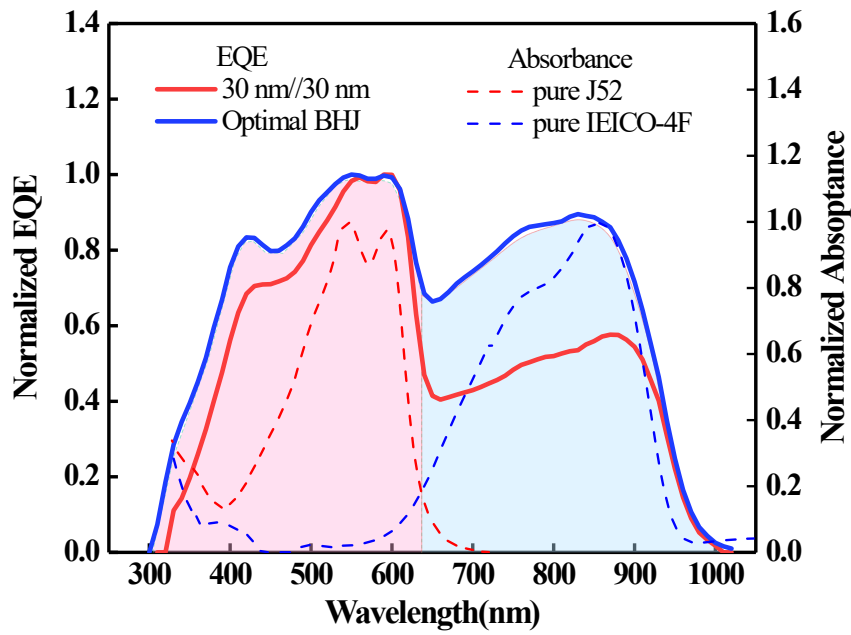


Fig. S5 Comparison of normalized EQE spectra (solid line) between PHJ and BHJ, showing apparent imbalance between short-wave region and long-wave region for PHJ. And both EQE spectra show a secondary peak for both EQE at the trough of the absorption spectra of the pristine film (dashed line).

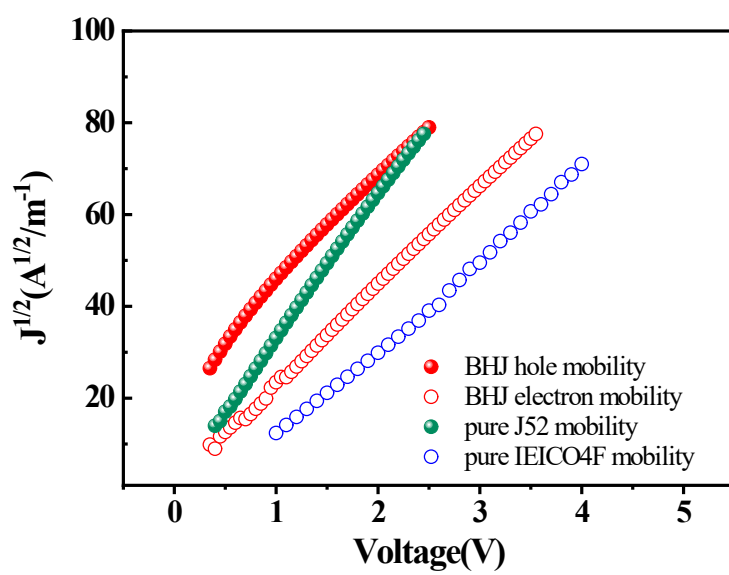


Fig. S6 $J^{1/2}$ -vs V plots, hole mobility for BHJ (red solid circle) and pure J52 film (green solid circle), electron mobility for BHJ (red hollow circle) and pure IEICO-4F film (blue hollow circle)

3. Supplementary Notes

3.1 Supplementary Note 1. |

3.1.1 Solving the generation charge generation efficiency at the interface η_{gen}

Following the paper by Schopp et al (Ref.7) , we performed geminate prefactor (P_g , which is the ratio between experimentally determined saturated photocurrent $J_{ph,sat}$ and the theoretical maximum short-circuit current $J_{sc,theo}$) analysis on our devices. Integrating $G(x, \lambda)$ over the active layer thickness, which means all excitons create free charge carriers, can yield the theoretical maximum short-circuit current $J_{sc,theo}$ ⁷, i.e. $J_{sc,theo} = q \int_L G(x) dx$. It doesn't hold in practice because of recombination. Here, the experimental saturated photocurrent $J_{ph,sat}$, which is reached at large reverse bias and so overcomes non-geminate recombination, is compared with $J_{sc,theo}$ to determine geminate prefactor P_g ²⁰, where $P_g = J_{ph,sat} / J_{sc,theo} = \eta_{ED} \eta_{gen}$. Moreover, by selective excitation on acceptor or donor, the corresponding geminate prefactor $P_g^{D,A}$, as well with η_{gen}^D and η_{gen}^A can be extracted if $\eta_{ED}^{D,A}$ is also known (here is set to unity as indicated above). **Fig.4a,b** depicts the photocurrent and the exciton generation rate distribution of BHJ device when only the donor or acceptor is excited, which can be used to calculate $P_g^{D,A}$. Here in this work, when only the donor is excited, $J_{sc,theo} = q \int_L G(x) dx = 10.98 \text{ mA/cm}^2$ and $J_{ph,sat} = 9.83 \text{ mA/cm}^2$, so $P_g^D = \eta_{gen}^D = 89\%$, namely the generation efficiency of charge in donor is 89%. Similarly, when only the acceptor is excited, $J_{sc,theo} = q \int_L G(x) dx = 14.42 \text{ mA/cm}^2$ and $J_{ph,sat} = 12.61 \text{ mA/cm}^2$, so $P_g^A = \eta_{gen}^A = 88\%$.

3.1.2 Solving the exciton diffusion efficiency for PHJ based on J-V curve and exciton generation rate profile

Similarly, geminate prefactor $P_g^{D,A}$ for the PHJ device can be achieved. The data shown in **Fig.4c,d** correspond to excitation of sole donor or sole acceptor in the same PHJ device. When only donor is excited, $J_{sc,theo} = 5.31 \text{ mA/cm}^2$, $J_{ph,sat} = 1.70 \text{ mA/cm}^2$, so $P_g^D = 32\%$. With $\eta_{ED}^D = 39\%$, charge generation efficiency $\eta_{gen}^D = P_g^D / \eta_{ED}^D = 82\%$. Similarly, when only acceptor is excited, $\eta_{ED}^A = 22\%$, $J_{sc,theo} = 8.08 \text{ mA/cm}^2$, and $J_{ph,sat} = 1.52 \text{ mA/cm}^2$, so $P_g^A = 18.5\%$ and $\eta_{gen}^A = 84\%$.

3.1 Supplementary Note 2. | Solving the exciton diffusion efficiency based on modeling the PL spectra of PHJ film

PL measurement: A pure J52 film, a pure IEICO-4F film, a BHJ film and a PHJ film are measured the Photoluminescence (PL) spectra by a Fluorolog-3 (HORIBA) spectrometer, respectively. We set the pump wavelength as 520 nm and 850nm to excite the J52 part and IEICO-4F part, respectively. In order to detect the PL response exceeding 1050nm, we use a NIR InGaAs detector to measure the PL signal.

PL spectra of pure donor (acceptor) and PHJ film are depicted in **Fig.3b**. We can see that excitation of J52 in PHJ film at 520nm yields a PL signal with two peaks, where J52's part declines significantly compared to the singlet exciton PL signal but visible emission from the IEICO-4F arises, indicating the existence of FRET from J52 to IEICO-4F. In other words, the IEICO-4F layer plays a role of quenching excitons in donor layer on one side, and can also absorb the energy from donor to yield

emission on the other side. Then we can solve η_{ED}^D and η_{ED}^A based on the data in **Fig.3b**. Compared with pure IEICO-4F film, the PL signal of PHJ excited by 850nm laser is reduced by about 23%, which is only originated from the reduction of excitons generated in the acceptor without concerning FRET effect. It means that the formation of PHJ quenches about 23% excitons in acceptor, again consistent with $\eta_{ED}^A=22\%$. In contrast, the formation of PHJ interface is enough to quench more than 90% excitons generated in donor. However, it doesn't mean $\eta_{ED}^D=90\%$ because some photons emitted by J52 are directly absorbed by IEICO-4F due to the large overlap between PL spectra of J52 and absorption spectra of IEICO-4F (see **Fig.1b**). Then another part of photons is quenched by the diffusion and dissociation of excitons of J52, which is related to η_{ED}^D .

The specific calculation process is as follows:

1. PL spectra of pure J52 film when excited by a 520nm laser is denoted as $PL_D(\lambda)$;
2. When 520nm laser pulse hits the PHJ film, on the one hand, part of excitons is quenched by the diffusion and separation and we denote the ratio as η_{ED}^D , so the reduced part is $\eta_{ED}^D * PL_D(\lambda)$. On the other hand, part of light emitted by J52 is directly absorbed by IEICO-4F and we denote the ratio as η_{ENTR} . So the reduced part is $(1-\eta_{ED}^D) * \eta_{ENTR} * PL_D(\lambda)$. So the remaining PL spectra of J52 is: $(1-\eta_{ED}^D)(1-\eta_{ENTR})PL_D(\lambda)$.
3. Photons of PL of J52 is absorbed by IEICO-4F, resulting in a $PL_A(\lambda)$ signal emitted by IEICO-4F. This absorbed part totally comes from the reduced

part of $(1-\eta_{ED}^D)*\eta_{ENTR}*PL_D(\lambda)$. So we can find the number of photons absorbed. Combined with the PL spectra of excitation of 850nm laser, we can solve the actual $PL_A(\lambda)$ because PL efficiency is constant.

4. It is important to note that this signal is meanwhile quenched by the exciton diffusion and separation because of the existence of PHJ interface.

Therefore, the remaining part is $(1-\eta_{ED}^A)*PL_A(\lambda)$.

5. Finally, the modeled PL spectra of PHJ can be expressed as:

$PL_{PHJ}(\lambda)=(1-\eta_{ED}^D)(1-\eta_{ENTR})PL_D(\lambda)+(1-\eta_{ED}^A)PL_A(\lambda)$, where η_{ED}^A is known and we only need to fit the measured PL spectra of PHJ to get the η_{ED}^D and η_{ENTR} .

Based on these analysis, we can obtain both η_{ED}^D and η_{ED}^A simultaneously, where $\eta_{ED}^D=39\%$ and $\eta_{ED}^A=22\%$ respectively, by modeling the PL spectrum of PHJ film considering the FRET effect. This result corresponds exactly to the diffusion efficiency value mentioned above, which proves the feasibility of this method.

3.2 Supplementary Note 3. | Solving the exciton diffusion length and charge generation efficiency simultaneously⁸

Generally, the exciton diffusion equation can be described by

$$\frac{\partial n}{\partial t} = D \frac{\partial^2 n}{\partial x^2} + G(x, t) - k_{PL}(t)g_t - k_{FRET}(x)g_t - \alpha g_t^2 \quad \text{eq-S1}$$

where n denotes the density distribution of singlet excitons at position x in the donor or acceptor layer, D the diffusion coefficient, and $G(x, t)$ the time dependent exciton

generation profile. The radiative decay rate in absence of quencher sites is k_{PL} , whereas k_{FRET} denotes the rate of Förster resonance energy transfer (FRET) in presence of a neighboring material with equal or smaller optical gap. α quantifies the rate for exciton–exciton annihilation. Based on some multiple simplifications including $\frac{\partial n}{\partial t} = 0, k_{PL} = \frac{D}{l_d^2}, \alpha = 0, k_{FRET} = 0$, we can simplify the steady-state equation as

$$G(x) = D \left(\frac{1}{l_d^2} - \frac{\partial^2}{\partial x^2} \right) n \quad \text{eq-S2}$$

where l_d is exciton diffusion length. In addition to exciton diffusion equation, exciton generation flux can also be obtained after calculation based on optical modeling as mentioned above. From ref.[7] we know that the exciton generation profile can be fitted with parabola approximation and the deviation does not exceed 3% for layer thicknesses up to 100nm. So we can fit the exciton profile with a typical quadratic function as

$$G_\lambda(x) = a_\lambda x^2 + b_\lambda x + c_\lambda \quad \text{eq-S3}$$

The exciton profile of each wavelength $G_\lambda(x)$ can be fitted independently and a set of corresponding $a_\lambda, b_\lambda, c_\lambda$ can be obtained. For example, as depicted in **Fig. 2d (inset)**, exciton generation profile of PHJ device can be obtained according to the calculation of optical modeling. We chose two wavelengths of 560nm and 800nm as an example, which solely excites donor layer and acceptor layer, respectively. All the profile can be fitted with parabolic approximation, especially for the thicker layer. Combine eq-S2 and eq-S3, we get

$$a_\lambda x^2 + b_\lambda x + c_\lambda = D \left(\frac{1}{l_d^2} - \frac{\partial^2}{\partial x^2} \right) n \quad \text{eq-S4}$$

After some reasonable assumption and simplifications, the photo-current originates from the flux of excitons diffusing from an absorption site in the donor ($i=D$) or acceptor ($i=A$) to their joint interface (D|A):

$$j_{photo} = q\eta_c(x_0) \sum_{i=D,A} D^i \left. \frac{\partial n_{D|A}^i(x_0, G^i, l_d^i)}{\partial x} \right| \quad \text{eq-S5}$$

whereas η_c represents the combined efficiency of charge generation (i.e. CT state splitting) and subsequent extraction of the charges at the designated electrode, x_0 is layer thickness.[14] Thus, besides charge extraction, j_{photo} strongly depends on the spatial distribution of excitons in both absorbers.

In earlier studies where bilayer solar cells with thin absorber layers were considered, the optical field within one absorber was simplified as constant: $G^i(x) \approx G_0^i$. In this *most simple case* (furthermore $\alpha = 0, k_{FRET} = 0$) the photo-current can be expressed as

$$j_{photo} \approx q\eta_c(x_0) \sum_{i=D,A} G_0^i l_d^i \tanh(f_{BC}^i x_0 / l_d^i) \quad \text{eq-S6}$$

Combining eq-S4 and eq-S6, we can finally get the photo-current

$$j_{photo} = l_d \left[\tanh \frac{x_0}{l_d} (G_\lambda(x_0) + 2a_\lambda l_d^2) + b_\lambda l_d \left(1 / \cosh \left(\frac{x_0}{l_d} \right) - 1 \right) - 2a_\lambda x_0 l_d \right] q\eta_c \quad \text{eq-S7}$$

where all orders of the optical field are now coupled to exciton diffusion. Moreover, j_{photo} of each wavelength can be obtained by EQE spectra and then we obtain an analytical expression for the photocurrent as a function of l_d and η_c . And has been obtained from the BHJ's calculation. Eventually, we can use eq-S7 to fit j_{photo} under

variation of wavelength λ and layer thickness x_0 , thus obtain I_d .

3.3 Supplementary Note 4. | Demonstrating Langevin reduction factor ζ based on a CT model

According to the work of McGehee's group⁹ and Madsen's group¹⁰, after excitons separate into free charges at the heterojunction interface, the electron and hole can meet at the interface again and form a CT state, which then either recombines or dissociates back into free carriers, which implies there is an equilibrium between charge transfer (CT) states and free carriers if CT states split much faster than they recombine. Moreover, this equilibrium is related to the ubiquitous reduced Langevin recombination observed in organic solar cells, as well as the open circuit voltage. Based on the fact that the CT state is in equilibrium with free carriers, we can assign the Langevin reduction factor in the framework of CT model to the expression of eq 2, where E_b is the binding energy of the CT state, where $E_b = E_{DA} - E_{CT}$ and E_{DA} is the effective band gap, $E_{DA} = E_L^A - E_H^D$, where E_L^A , E_H^D denote the positions at the interface of the LUMO level of the acceptor and the HOMO level of the donor, respectively. E_{CT} is 1.08eV from the EL spectrum of J52:IEICO-4F in our previous work.¹¹ σ_{CT} is the energetic disorder of CT state distribution, N_0 is the effective density of states. We consider these parameters

between PHJ and BHJ are equal since they share the same active layer materials¹².

The parameters used to calculate in eq 2 is listed in table S1.

Table S1. Parameters used to calculate the Langevin reduction factor in eq 2 and eq 3.

	E_{DA} (eV)	E_{CT} (eV)	E_b (meV)	σ_{CT} (meV)	N_0 (cm ⁻³)	k_L (cm ³ s ⁻¹)	f	V_{oc} (V)
BHJ	1.12	1.08	40	52	10 ²⁰	5.68×10 ⁻¹¹	0.9	0.68
PHJ	1.12	1.08	40	52	10 ²⁰	5.68×10 ⁻¹¹	0.03	0.72

References

- 1 C. Shuttle, B. O'regan, A. Ballantyne, J. Nelson, D. Bradley, J. De Mello and J. Durrant, *Appl. Phys. Lett.*, 2008, **92**, 80.
- 2 T. Kirchartz, B. E. Pieters, J. Kirkpatrick, U. Rau and J. Nelson, *Phys. Rev. B*, 2011, **83**, 115209.
- 3 T. Kirchartz and J. Nelson, *Phys. Rev. B*, 2012, **86**, 165201.
- 4 D. Credgington, S.-W. Liu, J. Nelson and J. R. Durrant, *J. Phys. Chem. C*, 2014, **118**, 22858-22864.
- 5 L. A. Petterson, L. S. Roman and O. Inganäs, *J. Appl. Phys.*, 1999, **86**, 487-496.

-
- 6 G. F. Burkhard, E. T. Hoke and M. D. McGehee, *Adv. Mater.*, 2010, **22**, 3293-3297.
 - 7 N. Schopp, V. V. Brus, J. Lee, G. C. Bazan and T.-Q. Nguyen, *Adv. Energy Mater.*, 2021, **11**, 2002760.
 - 8 B. Siegmund, M. T. Sajjad, J. Widmer, D. Ray, C. Koerner, M. Riede, K. Leo, I. D. Samuel and K. Vandewal, *Adv. Mater.*, 2017, **29**, 1604424.
 - 9 T. M. Burke, S. Sweetnam, K. Vandewal and M. D. McGehee, *Adv. Energy Mater.*, 2015, **5**, 1500123.
 - 10 Y. Liu, K. Zojer, B. Lassen, J. Kjelstrup-Hansen, H.-G. Rubahn and M. Madsen, *J. Phys. Chem. C*, 2015, **119**, 26588-26597.
 - 11 W. Wang, B. Zhao, Z. Cong, Y. Xie, H. Wu, Q. Liang, S. Liu, F. Liu, C. Gao and H. Wu, *ACS Energy Lett.*, 2018, **3**, 1499-1507.
 - 12 Z. Zheng, N. R. Tummala, T. Wang, V. Coropceanu and J.-L. Brédas, *Adv. Energy Mater.*, 2019, **9**, 1803926.